Submitted to Astrophysical Journal Letters August 5, 1998
Preprint typeset using LaTeX style emulateapj v. 04/03/99

MAPPING THE CMB I: THE FIRST FLIGHT OF THE QMAP EXPERIMENT

M. J. Devlin[1,2], A. de Oliveira-Costa[2,3], T. Herbig[2,4], A. D. Miller[2], C. B. Netterfield[5,2], L. Page[2] & M. Tegmark[3,4]

Submitted to Astrophysical Journal Letters August 5, 1998

ABSTRACT

We report on the first flight of the balloon-borne *QMAP* experiment. The experiment is designed to make a map of the cosmic microwave background anisotropy on angular scales from $0.^\circ 70$ to several degrees. Using the map we determine the angular power spectrum of the anisotropy in multipole bands from $\ell \sim 40$ to $\ell \sim 140$. The results are consistent with the Saskatoon (SK) measurements. The frequency spectral index (measured at low ℓ) is consistent with that of CMB and inconsistent with either Galactic synchrotron or free-free emission. The instrument, measurement, analysis of the angular power spectrum, and possible systematic errors are discussed.

Subject headings: cosmic microwave background – cosmology: observations

1. INTRODUCTION

Measurements of the anisotropy of the cosmic microwave background (CMB) are an effective probe of the state of the universe roughly 300,000 years after the big bang (White, Scott, & Silk 1994, Bond 1996). The anisotropy in the CMB not only provides a key test of models of structure formation, but analysis of its power spectrum may determine values of fundamental cosmological parameters such as Ω_0, H_0, and Ω_b.

The anisotropy in the CMB is measured with a variety of detectors and observing strategies (Bennett et al. 1997, Page 1997). QMAP was designed to directly produce a degree scale map of the sky that could be analyzed for anisotropy. In this paper, we report on the QMAP instrument and the first of two balloon flights. We present maps of the microwave sky and determinations of the angular power spectrum covering scales between 9° to $0.^\circ 7$ in two frequency bands centered on 31 and 42 GHz. An analysis of the second flight, systematic effects and calibration is presented in Herbig et al. (1998, hereafter H98), and the data analysis methods are described in detail in de Oliveira-Costa et al. (1998, hereafter dO98) together with results from combining the flights.

2. INSTRUMENT

The QMAP balloon-borne telescope was designed, built and flown twice in a period of 20 months. It consists of a cryogenic receiver, primary and secondary optics, pointing system, and data acquisition system.

The receiver, which was cooled to 2.3 K in flight, has four feed horns; one at Ka-band (31 GHz) and two at Q-band (42 GHz) each with 6-7 GHz of bandwidth [6]. Each Ka-band and Q-band band feed horn has two HEMT-based (high electron mobility transistor) amplifiers (Pospieszalski 1992), one in each polarization. These have been fully characterized and are described in Wollack et al. (1997) and Monnelly (1996). To account for the variable temperature and consequential gain drifts of the receiver, a thermally stabilized noise source calibrates all HEMT channels every 100 seconds with a 54 ms pulse. The noise power spectrum of each of the channels used in the final analysis is shown in Figure 1. The final map, discussed in Section 4.2, is based on the total sensitivity of the instrument, corresponding to the inverse quadrature sum of all of the detector noise power spectra.

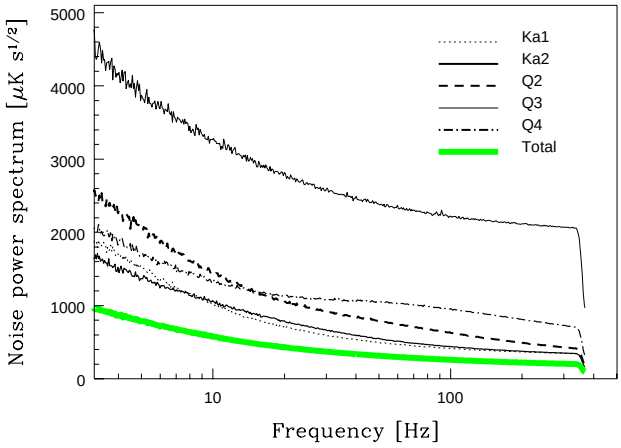

FIG. 1.— Noise power spectra of each of the channels that were used in the final analysis. The bottom curve is the inverse quadrature sum of all the channels.

The telescope optics are similar to those used for three ground based observations in Saskatoon, SK (Netterfield et al. 1997; Wollack et al. 1997). The telescope is mounted on an attitude-controlled balloon platform. The beams are

[1]Dept. of Physics, University of Pennsylvania, Philadelphia, PA 19104
[2]Dept. of Physics, Princeton University, Princeton, NJ 08544
[3]Institute for Advanced Study, Olden Lane, Princeton, NJ 08540
[4]Hubble Fellow
[5]California Institute of Technology, MS 59-33, Pasadena, CA 91125

[6]Though we flew a forth feed horn with a low noise 144 GHz SIS receiver (Kerr et al. 1993), it did not work on either flight. The problem was traced to a faulty LO in the first flight and remains undiagnosed in the second flight. The system now works in the ground-based MAT experiment. Also, HEMT amplifiers have improved considerably since this time (Pospieszalski et al. 1997)

formed by cooled corrugated feeds which under-illuminate an ambient temperature 0.85 m off-axis parabolic reflector which in turn under-illuminates a 1.8 m×1.2 m chopping flat mirror. The close-packed array of feeds form $0.^{\circ}89 \pm 0.^{\circ}03$, $0.^{\circ}66 \pm .^{\circ}02$ and $0.^{\circ}70 \pm 0.^{\circ}02$ beams for Ka1/2, Q1/2, and Q3/4 respectively. The beams are moved on the sky rapidly ($\approx$ 4.7 Hz) by the computer controlled resonant chopping flat which requires $\approx$ 20 W to operate. The output of the detectors are AC coupled and sampled 160 times during each chopper cycle. This rate is intended to adequately oversample the sky when the beam is moving at its fastest rate. The center of the $2.^{\circ}7 \times 2.^{\circ}7$ array was fixed at an elevation of $40.^{\circ}7$ for the first flight and $40.^{\circ}1$ for the second flight. The telescope is inside a large aluminum ground screen which is fixed with respect to the receiver and mirrors.

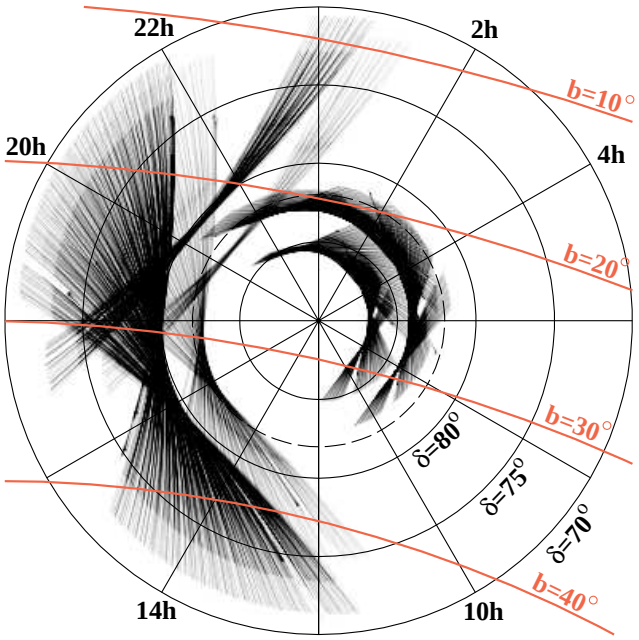

FIG. 2.— Sky coverage for flight 1 (left) and flight 2 (right) with intensity proportional to the time spent per pixel. Breaks in the coverage are due to calibrations. The scan paths are shown for all beams. For flight 1, Q3/4 are nearer the NCP (center of plot). SK observed the region inside the dashed circle.

The gondola is designed to be small, lightweight and rugged. This allows us to use a smaller, more manageable balloon which increases the probability of a successful launch and reduces the solid angle subtended by the balloon. The package was recovered from both flights with virtually no damage and is currently being used on a similar ground-based observation in Chile [7].

The attitude control system obtains primary pointing information from either a magnetometer or a CCD based star camera. When in CCD mode, the centroid of the chosen guide star in the CCD field is found in real time. This information is fed into a PID loop which controls the torque applied to a reaction wheel at the bottom of the gondola. Since the Ka/Q band receivers are relatively insensitive to pendulation induced atmospheric signals, no active elevation stabilization is required. This straightforward pointing system allows us to achieve good observing efficiency. During the first flight we integrated for 4.7 hours with no interruptions or pauses. A detailed description of the pointing system can be found in Beach (1996).

3. OBSERVATIONS

The payload was flown on June 16, 1996 from Palestine, TX and November 8, 1996 from Ft. Sumner, NM. Using a 4 mcf balloon, observations were made from an altitude of 30 km. In both flights, the entire instrument functioned nominally.

To produce high-quality maps from the data, a pixel should be referenced to its neighbors over multiple time scales, directions, and angular separations (Wright 1996, Tegmark 1997). This allows one to connect each pixel to many others and remove inevitable instrumental drifts and offsets in the data analysis. Our strategy is to sweep the beams horizontally with a 20° peak-to-peak amplitude at 4.7 Hz. In addition, the entire gondola is sinusoidally wobbled, about the meridian containing the NCP, with a peak-to-peak amplitude of 10° with a period of 100 seconds. As the flight progresses, one covers the sky as shown in Figure 2. In each sweep, $\theta_{throw}/\theta_{beam}$ is 20 and 30 for the Ka and Q-band, respectively (with $\theta_{throw}/\theta_{beam} < 10$, one has difficulty distinguishing features in the angular spectrum). A pixel is re-observed on time scales of 0.23 s from the chop, 100 s from the wobble, 12 minutes between the upper and lower beams, and $\approx$ 2 hours from the rotation of the earth. With a single long flight, or multiple shorter flights, a pixel is referenced to its neighbors in orthogonal directions. The chop and wobble amplitudes were reduced by approximately a factor of two for the second flight to increase the integration time per pixel. However, the basic scan strategy remained the same.

4. ANALYSIS

4.1. *Data Reduction and Calibration*

For the channels used in the analysis, there are no cuts to the data, no glitches were removed, and there is no detected interference from any on-board component [8]. A total of 12,884,480 temperature measurements were obtained in each channel. Removal of the internal calibration every 100 seconds reduced this by 4.8%. A time-independent radiometric offset of 10-15 mK (peak-to-peak) was present in all channels during the first flight. Much of this offset was traced to gap in the chopper baffle. For the second flight the offset was 1-2 mK (part of the reduction is due to a factor of two smaller chop angle). In both cases the offset is removed from each channel as described in H98 and dO98. The absolute pointing is determined during observations of Cas-A. With the pointing solution, the data are binned on the sky and analyzed as a map. The data are calibrated using Cas-A as described in H98.

[7] see http://dept.physics.upenn.edu/cmb.html and http://pupgg.princeton.edu/∼cmb/welcome.html for more information about the telescope in its balloon and ground-based configurations.

[8] Q1 was not used in the first flight due to interference for two hours and Q3 lost one stage of amplification.

4.2. *Map Production*

Making a map by simply averaging the observations in each sky direction would be inappropriate for two reasons: scan-synchronous offsets would cause artifacts, and $1/f$-noise would make the map unnecessarily noisy. We therefore adopted a more sophisticated approach, summarized below and described in detail in dO98.

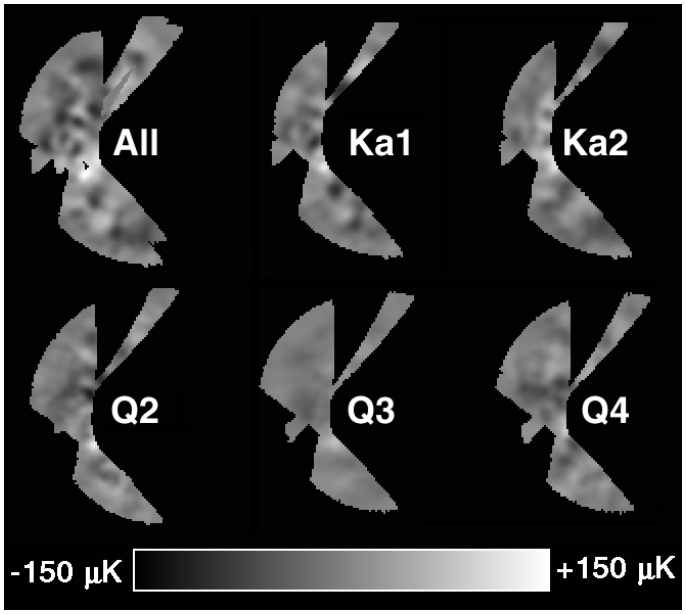

FIG. 3.— Wiener-filtered maps from flight 1. The CMB temperature is shown in coordinates where the NCP is near the center of each map, with RA being zero at the top and increasing clockwise.

The synchronous offsets, predominantly at the chopper frequency and the first overtone add mK-level signals to the map. This signal is eliminated by convolving the data with a notch filter that vanishes at these two frequencies, creating a data set completely independent of these offset harmonics and any slow variation in their amplitude. We choose this convolution filter to eliminate the DC component as well, and use the remaining degrees of freedom in the filter to render the filtered noise as close to white as possible. This produces a data set where each element is the sum of three terms:

1. A known linear combination of the actual sky temperatures;

2. A known linear combination of the higher-frequency synchronous offset, which we assume is constant; and

3. filtered detector noise, whose correlations vanish for time separations exceeding $\sim 10^2$ samples.

In other words, we have a greatly overdetermined system of linear equations. The map we compute is the solution to this linear inversion problem that minimizes the map noise, as described in dO98. For each of the five channels, the result of the mapmaking process is an N-dimensional map vector $\mathbf{x}$ (containing the temperature at each of the N pixels) and an $N \times N$-dimensional covariance matrix $\mathbf{\Sigma}$ which characterizes the pixel noise.

Wiener filtering is a useful tool for visualizing the data. It suppresses the noisiest modes in a map and shows signal that is statistically significant. The Wiener-filtered versions of our maps are shown in Figure 3 and are given by $\mathbf{x}_w \equiv \mathbf{S}[\mathbf{S}+\mathbf{\Sigma}]^{-1}\mathbf{x}$, where $\mathbf{S}$ is the covariance matrix corresponding to the level of sky fluctuations that we find in the data.

4.3. *Map tests*

A generalized χ^2-test for ruling out the null hypothesis that a given map contains no signal, merely noise, is discussed in dO98. Applying this test to the Ka1, Ka2, Q2, Q3 and Q4 channels shows that that signal is detected at the significance level of 17σ, 8σ, 5σ, 0.4σ and 3σ, respectively. To test whether this significant signal is common to the maps or due to systematic errors, we apply the same test to weighted difference maps of the form $\mathbf{x} \equiv \mathbf{x}_1 - r\mathbf{x}_2$ for different relative weights r. The comparison of Ka1 with Ka2 is shown in Figure 4, and it is seen that they pass three independent tests: $\mathbf{x}$ is inconsistent with noise both for $r = 0$ and $r = \infty$ (in which case only Ka1 or only Ka2 are probed), but perfectly consistent with noise for $r = 1$ (which gives the difference map Ka1-Ka2). Likewise, we find no evidence of any signal in the Q-band difference maps.

To see whether the signal can be accounted for by galactic foregrounds, we use this test to compare the Ka-band maps to those in the Q-band, writing $r = (\nu_{Ka}/\nu_Q)^\beta$. As seen in Figure 4, this places a 2σ lower limit on the spectral index β of -1.4, which means that the signal cannot be explained by foregrounds such as free-free emission ($\beta \sim -2.15$) or synchrotron radiation ($\beta \sim -2.8$) alone. For the CMB, $\beta = 0$.

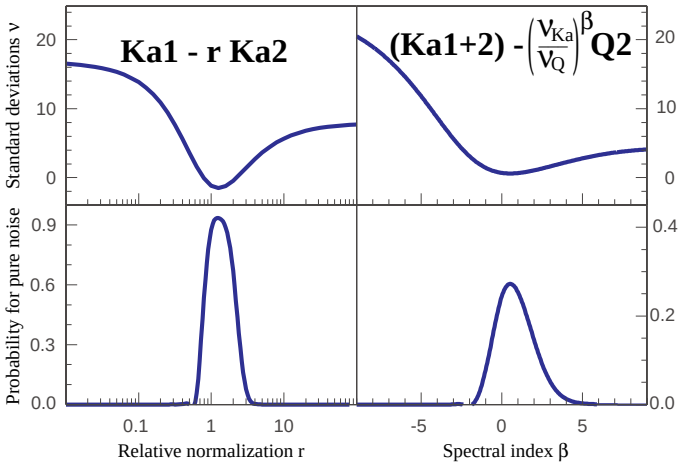

FIG. 4.— Evidence for common signal in the maps. The number of σ at which signal is detected in the weighted difference maps $\mathbf{x}_1 - r\mathbf{x}_2$ is shown (top) together with the corresponding probability that pure noise would give such a large χ^2-value (bottom). For maps at different frequencies (right), the spectral index $\beta = \ln r / \ln[\nu_{Ka}/\nu_Q]$ is constrained.

4.4. *Angular Power Spectrum*

We compute the angular power spectrum by expanding our maps in signal-to-noise eigenmodes (Bond 1995, Bunn and Sugiyama 1995); weight vectors $\mathbf{w}$ that solve the generalized eigenvalue equation $\mathbf{S}\mathbf{w} = \lambda\mathbf{\Sigma}\mathbf{w}$. When the $\mathbf{w}$ are sorted by decreasing eigenvalue λ, they tend to probe from larger to smaller angular scales. We obtain a statistically

independent power estimate from each mode, then average these individual estimates with inverse-variance weighting to obtain the band power estimates shown in Figure 5. For more details, see dO98.

5. CONCLUSIONS

The first QMAP flight has produced a 441 square degree map of the microwave sky at an angular resolution of $\sim 0.^\circ 7$, detecting sky signal that is statistically significant at $> 15\sigma$. Systematic checks confirm that the signal is fixed on the sky and not of instrumental origin. Spectral analysis shows that the dominant fluctuating component is the CMB. A future paper will address possible levels of contamination by foreground emission. This measurement is consistent with the Saskatoon results (Netterfield et al. 1997).

We gratefully acknowledge the contribution and support of many people associated with this project. Norm Jarosik provided valuable insights and beautiful electronics. Dave Wilkinson and Steve Meyer provided many useful discussions. Marian Pospieszalski and Mike Balister of NRAO provided the HEMT amplifiers without which this experiment would not have been possible. The staff at the National Scientific Balloon Facility provided invaluable support for our flights. We also thank Jed Beach, Stuart Bradley, Chris Gable, Glen Monnelly, Andrea Wood, and the Princeton University Machine Shop for their help in constructing the apparatus, and Suzanne Staggs for helpful comments on the manuscript. The window functions are available at the web sites[7], where the calibrated raw data with pointing will be made public after publication of this *Letter*.

This work was supported by a David & Lucile Packard Foundation Fellowship (to LP), a Cottrell Award from Research Corporation, an NSF NYI award, NSF grants PHY-9222952 and PHY-9600015, NASA grant NAG5-6034 and Hubble Fellowships HF-01044.01−93A (to TH) and HF-01084.01−96A (to MT) from by STScI, operated by AURA, Inc. under NASA contract NAS5-26555.

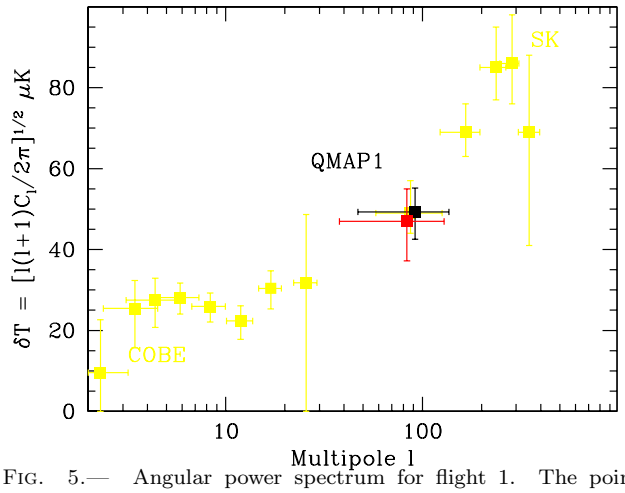

FIG. 5.— Angular power spectrum for flight 1. The point on the left is for the Q-band and corresponds to the band power $\delta T_\ell = [\ell(\ell+1)C_\ell/2\pi]^{1/2} = 47^{+8}_{-10}$ μK in a window whose mean and rms width is given by $\ell = 84 \pm 46$. The point on the right is for the Ka-band and corresponds to $\delta T_\ell = 49^{+6}_{-7}$ μK in a window $\ell = 92 \pm 45$. These error bars do not include a calibration error of 12% and 11%, respectively.

REFERENCES

Beach, J. 1996, Senior Thesis, Princeton University
Bennett, C. L. , Turner, M. S., White, M. 1997, Physics Today, 50:11, 32
Bond, J. R. 1995, Phys. Rev. Lett., 74, 4369-4372
Bond, J. R. 1996 *Theory and Observations of the Cosmic Microwave Background Radiation*, in "Cosmology and Large-Scale Structure", Les Houches Session LX, August 1993, ed. R. Schaeffer, Elsevier Science Press
Bond, J. R., Efstathiou, G., Tegmark, M. 1997, MNRAS, 291, L33-41
Bunn, T., Sugiyama, N. 1995, ApJ, 446, L49-52
de Oliveira-Costa, A. 1998, astro-ph/9808045
Herbig, T., et al. 1998, astro-ph/9808044
Kerr, A. R., Pan, S.-K., Lichtenberger, A. W., and Lloyd, F. L. 1993, Proceedings of the Fourth International Symposium on Space Terahertz Technology, pp 1-10.
Monnelly, G. 1996, Senior Thesis, Princeton University
Netterfield, C. B., et al. 1997, ApJ, 474, 47-66
Page, L. A. 1997, Generation of Large-Scale Structure, Eds D. N. Schramm and P. Galeotti, (Kluwer, Netherlands), p75
Pospieszalski, M. W. 1992, Proc. IEEE Microwave Theory Tech., MTT-3 1369; erratum Pospieszalski, M. W. et al., Proc. IEEE Microwave Theory Tech., MTT-3, 1345 (1994)
Pospieszalski, M.W. 1997, Microwave Background Anisotropies (Ed. Frontieres, ed. Bouchet et al), pp 23-30
Tegmark, M. 1997, Phys. Rev. D, 56, 4514
White, M., Scott, D., & Silk, J. 1994 A&A, 32, 319-370
Wollack, E. J., Devlin, M. J., Jarosik, N.J., Netterfield, C. B., Page, L., Wilkinson, D. 1997, ApJ, 476, 440-447
Wright, E. 1996, astro-ph/9612006